ARTICLE

Bioactive Nanocomposite Coatings for Visible-Light Illumination Promoted Surface-Mediated Gene Delivery

Received 00th January 20xx,
Accepted 00th January 20xx

DOI: 10.1039/x0xx00000x

Lili Yao [a], Xiaozhao Wang [b], Wenjian Weng [a], Yongqing Fu [c] and Kui Cheng *[a]

Gene delivery based on bioactive coatings on collagen has great potentials for bone repair applications. Meanwhile, controlled gene delivery at specific times/regions is essential for an efficient and complete bone reconstruction process. However, spatio-temporal regulation of gene release and delivery remains a great challenge. In this paper, we used visible-light illumination to effectively regulate gene release and subsequent delivery into biological cells. A visible-light responsive and bioactive nanocomposite coating (based on collagen/gold-nanoparticles, *e.g.*, Col/AuNPs) was prepared through hydrothermal and sol-gel processes and used as a loading platform for complexes of enhanced green fluorescent protein and Lipofectamine2000 (LF/GFP). Results showed that the amount of immobilized LF/GFP was increased on Col/AuNPs and the release of pre-adsorbed LF/GFP was significantly enhanced in a spatio-temporal and controllable manner under the visible-light illumination. Moreover, the cellular intake of released gene was improved, thus enhancing gene expression efficiency of the cells. The mechanism of enhanced controlled gene delivery was attributed to the changes of collagen structures and rearrangement of cytoskeletal structures induced by the photothermal effect. The developed Col/AuNPs composite coating is effective for both controlled surface-mediated gene delivery and gene-mediated bone repair.

Introduction

Bioactive coatings play an important role in tissue repair and regenerative medicine, especially in repair and reconstruction of bone defects. [1-4] Various bioactive materials, such as bioceramics, synthetic or natural polymers and their composites, have been investigated as bioactive osteoconductive coatings. [5-8] Recently, growth factors such as bone morphogenetic protein-2 (BMP-2) and vascular endothelial grown factor (VEGF) were further loaded on these bioactive coatings, so that osteogenic differentiation of stem cells, which is found to be essential for bone regeneration, could be improved. [9-11] However, high doses of growth factors were generally needed due to their poor affinity to coatings and short half time in body, which may lead to complications such as ectopic bone formation and inflammation. [12] Expression of endogenous growth factors through gene transcription is regarded as one of the appropriate approaches to overcome the above problems. Nevertheless, before transcription, genes must be delivered to the targeted cells effectively. Hence, a reliable route to deliver the genes locally to the targeted tissues, such as surface-mediated gene delivery and reverse gene delivery which immobilize the genes onto surface before cell seeding, [13, 14] becomes a reasonable strategy for designing bone restoration biomaterials. [15]

However, efficient gene delivery at specific time/regions is still very challenging, but critical to clinical bone repair. [16] Generally, such delivery methods include effective immobilization and release of genes and intake of genes by the targeted cells. [17-19] Numerous studies have been carried out on immobilization and releases of the genes. For example, various methods such as electrostatic interaction, [20] hydrogen bonding [21] and covalent bonding [22] have been utilized to control the immobilization of genes. However, many of these control methods have difficulties in timely release of genes. [23] Various external driven forces, including those generated by changes of pH, temperature, electrical current/voltage and light intensity have been explored to promote the fast gene release. [24-29] For efficient cellular uptake of gene, most studies are focused on optimization of various viral or non-viral vectors, so that a balance between high delivery efficiency and safety could be reached. Alternatively, physical enhancement methods, such as

[a] School of Materials Science and Engineering, State Key Laboratory of Silicon Materials, Cyrus Tang Center for Sensor Materials and Applications, Zhejiang University, Hangzhou, 310027, China
[b] Department of Orthopaedic Surgery, Second Affiliated Hospital & Zhejiang University-University of Edinburgh Institute & School of Basic Medicine, Zhejiang University School of Medicine, Hangzhou 310058, China
[c] Faculty of Engineering & Environment, Northumbria University, Newcastle upon Tyne, NE1 8ST, United Kingdom
† Electronic supplementary information (ESI) available. See DOI:

electroporation, sonoporation and photoporation, have been widely investigated to promote cellular uptake of genes, through enhancing cell membrane permeability. [29-34] Recently, Wang et al. and Zhang et al. found that efficiency of surface-mediated gene delivery was enhanced due to the photothermal effect generated from polydopamine, [35, 36] proving that photothermal stimulation could influence gene delivery. Nonetheless, the degree of dopamine polymerization needs to be strictly controlled, otherwise it will cause biosafety issues.

In this work, we proposed a new idea to use bioactive coatings and combine with the visible-light illumination, in order to effectively deliver genes. Collagen (Col) was chosen as both the matrix of the coating owing to its effectiveness as bioactive ingredients and the loading platforms for osteogenic gene delivery in bone repair materials. [37-40] Biocompatible and photo-responsive gold nanoparticles (AuNPs) [41-43] were incorporated into collagen, in order to provide the coating with a capability to respond to visible-light. Moreover, a quartz glass with TiO_2 nanorods array (TiNR) was utilized as the substrate to prevent the coating from unwanted peeling-off. The photothermal properties of the composite coating and the conformation changes of collagen were characterized. Behaviors of gene release and gene delivery under the visible-light illumination were evaluated. Finally, the mechanism of visible-light regulated gene delivery using the composite coatings of collagen/gold-nanoparticles (Col/AuNPs) was proposed.

Results and discussion

Characterization of Col/AuNPs and Visible-light Illumination to Composite Coating

TEM image displays nearly spherical particles of prepared AuNPs with a diameter of about 20 nm (Figure S1a, ESI). The size of AuNPs measured by dynamic light scattering (DLS) is 23.9 ± 0.4 nm in diameter, which is larger than TEM analysis owing to the solvation and hydration of particles [44]. The zeta potential is 41.1 ± 2.4 mV, which indicate that the AuNPs are stable and resistant agglomerate (Figure S1b, ESI). And the size and zeta potential distribution of synthetic AuNPs are relatively uniform (Figure S1d and e, ESI). An obvious absorption peak of AuNPs is observed at 523 nm in the UV-Vis spectra of AuNPs solution, and the absorption peak of AuNPs still exist but have a minor red shift to 525 nm after collagen gel inclusion (Figure S1c, ESI). Similar phenomenon has been observed in previous research. [45] Figure 1a shows a typical morphology of the Col/AuNPs composite coating observed using a scanning electron microscope (SEM). The coating is quite dense, and elemental distributions of C and Au characterized using an energy dispersive X-ray spectroscope (EDS) confirmed that the AuNPs are homogeneously distributed inside the coating (Figures 1b and 1c). The widths of most TiNRs are about 100 nm (Figure S2, ESI). Cross-section observation of the Col/AuNPs coating shows that the lengths of TiNRs are about 480~520 nm, and the TiNRs are evenly distributed inside the Col/AuNPs matrix (Figure 1d). Such a structure is believed to be beneficial for improved coating adhesion through an effective mechanical interlocking mechanism.

Different concentrations of AuNPs were mixed uniformly in the collagen solution (e.g., 0 mg mL^{-1}, 0.17 mg mL^{-1}, 0.33 mg mL^{-1}, 0.50 mg mL^{-1} of AuNPs), and the corresponding coatings are named as TiNR/Col, Col/AuNPs-L, Col/AuNPs-M, Col/AuNPs-H, respectively. The photothermal behaviors of the coatings were characterized and the results are shown in Figure 1e. The temperature of TiNR/Col is increased slightly (1.3 ℃) after 15 min light illumination, and the temperature increment (△T) of Col/AuNPs is increased with the content of AuNPs (3.1 ℃ for Col/AuNPs-L, 3.5 ℃ for Col/AuNPs-M and 4.1 ℃ for Col/AuNPs-H, respectively). The value of △T is also increased with increasing light intensity, as shown in Figure 1f. Furthermore, the value of △T is increased rapidly with the increase of illumination time in the first three minutes, but the increase rate is significantly decreased with further illumination. These results indicate that Col/AuNPs possess good photothermal property and the photothermal conversion ability could be regulated by the content of AuNPs, light intensity and illumination time.

Thermal effect during the illumination could cause denaturation or even degradation of the collagen, [45] which would play an important role in regulating desorption of LF/GFP. Therefore, the secondary structures of collagen were characterized using Fourier transform infrared spectrometer (FTIR), in order to understand the effects of light illumination to collagen conformation. The fitted FTIR peaks (see Figure 1g and Table 1) show that the secondary structures of collagen underwent significant changes after light illumination. The content of triple helix structure is reduced from 21.6 % to 16.1 %, while the side chain structure is increased from 0.0 to 10.1 %. The ordered structures of α-helix (from 28.3 % to 18.7 %) and β-sheet (from 24.3% to 22.0 %) are both decreased, whereas the unordered structures of β-turn (from 16.7 % to 18.7 %) and unordered conformation (from 9.1 % to 14.4 %) are both increased. Results indicate that the thermal energy generated by visible-light illumination influences the conformation of collagen, manifested by the depolymerization of the tripe helix structure, exposure of side chains and formation of more disordered molecular chains.

The surface of Col/AuNPs composite coating is in direct contact with LF/GFP and cells, therefore, the changes of surface are crucial for gene release and cellular behaviors. In order to verify whether there is light-induced collagen conformation occurring on the surface, X-ray photoelectron spectroscope (XPS) was used to characterize the sample of Col/AuNPs. Figures 1h to 1i shows the C1s and N1s of C-containing and N-containing groups, which can be used to identify the existence of the collagens. The deconvolution results of C 1s and N 1s spectra indicate detailed information about collagen and are listed in Tables 2 and 3. Clearly, an evaluation of the deconvoluted C 1s components reveals that an increase in the amount of OC-NH (21.5 % to 27.9 %), a reduction in C-O/C-S (13.2 % to 7.6 %) and C-H (27.5 % to 21.3 %), and a slight increase in C-N (21.3 % to 23.6 %) and C-C (16.5 % to 19.6 %) for Col/AuNPs coating with illumination in comparison to those without illumination. Also, the fitted N 1s shows an increase in OC-NH (8.5 to 14.0 %) and C-N (34.6 % to 36.7 %), and a decrease in NH2 (39.9 % to 38.0

%) and -N= (17.0 % to 11.3 %). Such results imply that the N and C containing groups of collagens on the surface has been changed after the light illumination. Combined with the results of FTIR, it could be speculated that the changes of collagen conformations probably contributed to such changes on the surface.

The above results confirm that the Col/AuNPs composite coating shows obvious photothermal effect under the visible-light illumination. The thermal energy would change the conformation of collagen, which could influence the molecules immobilized on collagen and cellular responses.

Cell Responses to Col/AuNPs Composite Coating

Good cytocompatibility is one of the basic requirements for biomedical materials. Therefore, we have characterized the adhesion and proliferation behaviors of cells grown on Col/AuNPs. After cultured for 1 day, cells grown on the TiNR coating showed slightly circular morphology and poor cytoplasm extension. In contrast, cells grown on Col/AuNPs coating exhibited a spindle morphology and a significant cytoplasm extension (Figure S3a, ESI). Although optical density (OD) values of cells on Col/AuNPs were comparable to those on the TiNR coating after cultivation for 1 day and 3 days (Figure 2a), the better adhesion behavior in the early-stage for the cell growth revealed that the Col/AuNPs showed good property of cell viability over TiNR. In addition, no adverse effects were observed on number and spreading morphology of cells grown on Col/AuNPs composite coatings with different contents of AuNPs and with visible-light illumination (Figure 2a, Figure S3b-c, ESI).

The maintenance of biological function during the light illumination is critical for bioactive coatings. It was previously reported that the TiNR coating has good osteoconductive performance. [46] We have characterized the osteogenic differentiation behaviors of Col/AuNPs composite coating with/without light illumination. As a marker in the early differentiation stage, alkaline phosphatase (ALP) activities of cells on different samples were characterized and the results are shown in Figures 2b and 2c. All the three samples showed equivalent ALP activities at day 7 and day 14, indicating that cells on Col/AuNPs coating had a well osteogenic differentiation potential with or without light illumination.

To further probe the osteogenic differentiation of cells on the coatings, polymerase chain reaction (PCR) tests were carried out to analysis the osteogenic-related gene markers at the molecular level. The obtained results are shown in Figure 2d. For the expressions of ALP, Col- I and Runx-2, all samples show equivalent levels, whereas the expression level of osteocalcin (OCN) in day 7 on Col/AuNPs with light illumination was increased to 1.4-fold more than that on the TiNR. Such results implied that the composite coating and visible-light illumination have a slightly positive effect on osteogenic differentiation compared to TiNR.

These results clearly indicate that the Col/AuNPs composite coating and visible-light illumination showed similar cell viability and slightly improved osteogenic differentiation of the MC3T3-E1 cells.

Immobilization and Release of LF/GFP under Visible-light Illumination

Figure 3a shows results of Lipofectamine2000/pEGFP complexes (LF/GFP) immobilization on TiNR and Col/AuNPs, which is an important factor in regulating surface-mediated gene delivery. The obtained quantitative data indicates that the Col/AuNPs coatings effectively immobilize more LF/GFP than the bare TiNR coating, which is in a good agreement with the fluorescence results shown in Figure S4a (ESI). The release amount of LF/GFP was further obtained using the fluorescence quantitative analysis method after immersion in PBS for a specified time. It was observed that 80 % and 18 % of the LF/GFP were released from the TiNR and Col/AuNPs coatings after 48 h immersion (Figure 3b). The results clearly indicate that the presence of Col/AuNPs on top of the TiNR effectively inhibited the initial burst release of LF/GFP.

The intensity of the visible light illumination was found to effectively affect the release of LF/GFP. As shown in Figure 3c, significant increase of LF/GFP release was observed when the light intensity was increased to 150 mW cm^{-2}. Nevertheless, further increase of light intensity resulted in slight decrease of release. Such a decrease could be attributed to the degradation of collagens and their dispersion into supernatant, which intervened the detection of LF/GFP (Figure S4b, ESI). It was also found that the amount of released LF/GFP was increased with increasing illumination time (Figure 3d). Clearly, light illumination is an effective route to control the release of LF/GFP.

Generally, in surface mediated gene delivery, genes need to be released at the appropriate time after cells are attached on the surface, and thus it is crucial to control gene release in an on-demand and switchable manner. Figures 3e to 3f show the amount of LF/GFP release from Col/AuNPs coating after illumination at different times and with a periodic light illumination. The results revealed that, within the initial 48 h, the release of LF/GFP was notably enhanced at any time point with light illumination, in comparison with those without light illumination (Figure 3e). Fluorescent images of Col/AuNPs after LF/GFP release were further taken and are shown in Figure S5a (ESI), which display similar results. A large amount of LF/GFP remain attached to the surface of Col/AuNPs, even after release for 48 h without light illumination. However, only a small amount of LF/GFP was detected on the surface, when the Col/AuNPs coating was illuminated immediately after being transferred to fresh PBS. It is inevitable that few LF/GFP was detected on the composite coating when the Col/AuNPs coating was illuminated after being soaked in fresh PBS for 24 h/48 h. When the light cycle was set as 10 min (*e.g.*, light-on for 5 min and light-off for 5 min), the release of LF/GFP was slightly enhanced during the light-on stage than that during the light-off stage (Figure S5b, ESI). When the light cycle was set as 20 min (*e.g.*, light-on for 10 min and light-off for 10 min), the amount of released LF/GFP was significantly increased during the light-on stage, compared with that during the light–off stage (Figure 3f). All the above results implied that the release of LF/GFP could be regulated in a switchable manner.

A light mask (Figure S6a, ESI) was further deposited on the TiNR/Col and Col/AuNPs coatings to study spatial controllability of light-regulated release of LF/GFP. There are not obvious differences between light exposed area and unexposed area for the TiNR/Col. Whereas for Col/AuNPs, the amount of residual LF/GFP in the light exposed area was much less than that in the unexposed area (Figures S6b and c, ESI). Results clearly indicated that the release of LF/GFP on Col/AuNPs coating could be controlled in a spatial controlled manner.

In brief, the introduction of collagen and AuNPs into TiNR increases the amount of immobilized LF/GFP and hinders its release. Furthermore, the release of LF/GFP could be regulated in a space-time controllable manner with the visible-light illumination.

Effects of Visible-light Illumination on Cellular Endocytosis of LF/GFP

It was previously reported that the surface properties of biomaterial, including composition, [47] stiffness, [48] topography [49] and so on, could affect cytoskeletal rearrangement, thereby influencing its cellular endocytosis. [50] In order to investigate whether the photothermal properties of the composite coating could lead to cytoskeletal rearrangement, we have used the laser confocal microscope for this study. The obtained images clearly show that cells grown on the Col/AuNPs showed more elongated morphology and brighter fluorescence colour under light illumination, when compared with those without light illumination. Moreover, actin filaments of the cells are arranged in parallel (Figure 4a). Such rearrangement of the cytoskeleton is probably caused by the change of collagen conformation and directly photothermal heating. All the above phenomena indicated that more polymerized actin formed and cells have a stronger ability for cellular endocytosis to LF/GFP with the light illumination.

In conventional gene delivery process, gene load carriers are directly added to the cell culture mediums. Unlike surface-mediated gene delivery, it does not involve the release of gene load carriers, while cells directly endocytose the carriers from the surrounding medium. In order to study the effect of light illumination on cellular uptake of LF/GFP without the interference of the release of LF/GFP, the conventional gene delivery experiment was performed. The results obtained from a flow cytometry shown in Figure 4b indicate that the expression efficiency of green fluorescent protein (GFP) and mean fluorescence intensity with visible-light illumination are both increased by 1.2-fold, when compared with those without visible-light illumination. Fluorescence microscopy images in Figure 4c show the similar results, highlighting the positive effect of light illumination on cellular endocytosis of LF/GFP.

Clearly, photothermal process of Col/AuNPs coating under the visible-light illumination affected rearrangement of the cytoskeleton, then enhanced the cellular endocytosis of LF/GFP.

Effects of Visible-light Illumination on Gene Delivery Efficiency

As shown in Figure 5a, the measured amounts of GFP expressions for cells cultured on Col/AuNPs are obviously increased owing to the effective immobilization of LF/GFP. Moreover, applying visible-light illumination further improved the amount of expression of cells. Data measured from flow cytometry further accurately proved that the GFP expression efficiency of cells on Col/AuNPs was 2.1-fold as much as that on TiNR. The value was further increased to 2.6-fold after using the visible-light illumination (Figure 5b-c). Clearly, the rapid release of LF/GFP after using the visible-light illumination has contributed to the enhanced GFP expression. However, cytomembrane is still an inevitable barrier during biomolecule transport, and the enhanced cellular uptake of LF/GFP is another critical factor in enhancing gene expression efficiency.

It is worthwhile to note that the above obtained gene expression efficiency is lower than that obtained using the conventional method (Figure 4b). The reason can be attributed to that the amount of pEGFP released (about 90 ng well^{-1}) was less than that usage in the conventional method (200 ng well^{-1}). Moreover, the results obtained from the periodic light illumination experiments showed that the gene delivery efficiency in surface-mediated gene delivery was further enhanced through optimizing light illumination conditions. Such *in-situ* surface-mediated gene delivery is more efficient than the conventional gene delivery.

Above results demonstrated that visible-light illumination enhances surface-mediated gene delivery, and its mechanism is proposed and illustrated in Figure 6. On one hand, the structure of collagen becomes more disordered under visible-light illumination due to the photothermal effect in the composite coating. The disturbance of these collagen structures weakens the interaction between LF/GFP and coating surface, thus resulting in the rapid release of LF/GFP. On the other hand, the collagen conformation changes and photothermal heating induced by the photothermal effect of Col/AuNPs under light illumination trigger the rearrangement of cytoskeleton, which enhances the cellular intake of released LF/GFP. Eventually, the two processes synergistically regulated the surface-mediated gene delivery.

Surface-mediated *in vivo* gene delivery is quite challenging due to the inherent barriers in LF/GFP transport. In comparison with a single cell, cell sheets with a high cell density are abundant for interactions between cell and cell as well as cell and extracellular matrix, which is more applicable in mimicking *in vivo* gene delivery processes. To further assess the potential application of such light-regulated *in vivo* surface-mediated gene delivery, the experiment of gene delivery to cell sheets was further carried out. The cell sheets were obtained from silicon wafers with a p-n homojunction as reported in the literature [51] and the image of detached cell sheet is displayed in Figure 7a. After re-cultured on Col/AuNPs composite coatings for 2 days, there are few dead cells observed on these cell sheets (Figure 7b). The GFP expression efficiency was relatively low in cell sheets. That might be ascribed to the barrier effects of extracellular matrix and different cell status [52]. Nevertheless, light illumination significantly improved the GFP expression efficiency (Figure 7c). Such results clearly suggest that visible-light illumination has enhanced gene delivery efficiency in cell sheets and exhibit an excellent potential for *in vivo* applications.

Conclusions

In this study, the osteoconductive bioactive coating was prepared by incorporating Col/AuNPs into TiNR and was applied as a platform for LF/GFP loading. Visible-light illumination was used to regulate rapid surface-mediated gene delivery. Photothermal effects were observed through a simple illumination of a non-laser and cold light source. The collagen structure became more disordered due to the photothermal effect, and the disturbance of collagen structure induced rapid released of LF/GFP under light illumination. Furthermore, the thermal energy generated by light illumination could regulate cytoskeletal rearrangement, thus resulting in an enhanced cellular uptake capability. The cells grown on the Col/AuNPs showed significantly higher GFP expression efficiency with light illumination. The enhancing mechanism was attributed to the accelerated release of LF/GFP and enhanced cellular uptake ability, as well as synergistically controlled surface-mediated gene delivery. This work has created a new design methodology for the controlled surface-mediated gene delivery based on an osteoconductive bioactive coating. More importantly, it offered a new strategy for controllable gene-mediated bone repair by regulating the delivery of functional molecules into specific cells.

Experimental Section

Preparation and Characterization of Col/AuNPs Coatings

TiNR on the surface of substrate was prepared according to that reported in the previous publication. [53, 54] Briefly, a seed layers of TiO_2 nanodots were firstly prepared through a sol-gel method. Hydrothermal method was then used to prepare nanorods in a solution containing deionized water, concentrated hydrochloric acid and tetrabutyl titanate. Surfaces with such nanorod arrays were reported to have a good biocompatibility. [55] A mixed sol was obtained by dissolving type Ⅰ collagen (obtained from Beijing Yierkang, China) into AuNPs solution with acetic acid under a mild stirring. The final concentration of the mixed was set to be 0.2 wt% of collagen and 0.50 mg/mL of AuNPs. Col/AuNPs coatings was prepared through a spin-coating method: *e.g.*, 30 μL of the mixed sol was firstly dripped onto surface with TiNR, and then spun at 7000 rpm for 40 s. Surface and cross-section morphology of the coatings were observed using an SEM (Hitachi, SU47) with a 3.0 kV operating voltage. Element distribution of the coating was measured using the EDS attached with the SEM. Biological activity of composite coating was evaluated using different methods of cellular adhesion, proliferation and osteogenic differentiation. Detailed experimental processes are illustrated in Figure S7 (ESI).

Visible-light Illumination to Col/AuNPs Composite Coating

A halogen cold light source (Mingri Technique, XD-302, 400-800 nm) was used in this study. The light intensity was determined using a solar power meter (Xinbao Technique, SM306). During all the visible-light treatment processes, the cold visible-light is illuminated onto samples from above, and the schematic diagram of the lighting device is shown in Figure S8 (ESI). To study the photothermal performance of composite coatings, samples were exposed to visible-light at a certain intensity and time, and the temperatures were recorded using an infrared thermal camera (FLIR, E40). When analysing the effect of AuNPs content on △T, light intensity was set to be 150 mW cm^{-2}. Col/AuNPs-L was used as a typical sample to study the effect of light intensity on △T. Samples were characterized using FTIR (PerkinElmer, Spectrum 2000) and XPS (Kratos AXIS Ultra DLD) after light illumination at the intensity of 150 mW cm^{-2} for 15 min. The amplified FTIR spectra between 1600 cm^{-1}~1700 cm^{-1} (amine Ⅰ absorption) were used to study the changes of collagen conformation after curve fitting with the software of PeakFit. [56] The detailed XPS spectra of C 1s and N 1s were fitted using XPS Peak 4.1 software to analyse changes in surface chemical of coating, after the system was calibrated with C 1s (284.6 eV).

Immobilization and Release of LF/GFP

pEGFP (Genscript), a plasmid encoding GFP, was served as reporter gene and lipofectamine2000 (Invitrogen, Lipofectamine® 2000 Reagent) was used as gene vector in this study. The LF/GFP were prepared according to manufacturer's protocol. Briefly, lipofectamine2000 and pEGFP were incubated in phosphate buffered saline (PBS, pH 8.0, HyClone) at concentrations of 12 μL mL^{-1} and 4 μg mL^{-1}, separately, for 10 minutes, then the pEGFP solution was added dropwise to the lipofectamine2000 solution and incubated for another 5 minutes at room temperature. For immobilization of the LF/GFP, samples were placed in 24 well plates and soaked in 500 μL $well^{-1}$ of LF/GFP solution at 4 ℃ for 12 h immediately after LF/GFP formation. The final amount of the pEGFP was 1μg $well^{-1}$, and the ratio of pEGFP to lipofectamine2000 was 1μg/3μL within the usage range recommended by the manufacturer. The samples were gently washed twice with the PBS to remove unbound LF/GFP. The amount of pEGFP (which is used to represent the relative amount of LF/GFP) on the substrate was determined after staining with Helixyte Green (ATT Bioquest) and then analyzed using a fluorescence microscope (Nexcope, NIB900). The amount of pEGFP in supernatant was also quantified by a fluorescence microplate reader (MDS Analytical, M200) after labelled with Helixyte Green.

In order to study the spontaneous release of LF/GFP, samples with the LF/GFP loading were soaked in the fresh PBS at 37 ℃ in a humid chamber and a small amount of the solution was taken out at a specific time point (*e.g.*, 0 h, 0.5 h, 1 h, 2 h, 12 h, 24 h and 48 h) to determine the amount of released LF/GFP. For visible-light controlled release of LF/GFP, samples with LF/GFP loading were immersed in the PBS at 37 ℃ in a humid chamber, and then exposed to visible-light with predetermined conditions. After visible-light illumination, the supernatants were collected and the amount of released LF/GFP was quantified using the fluorescence microplate reader as mentioned above. The remaining amount of LF/GFP on substrates were analyzed using the fluorescence microscope as described above. In the periodic light on-off experiment, the supernatant was preserved and fresh PBS was added at the end

of each light-on or light-off stage. The collected supernatants were used to determine the amount of released LF/GFP during this period.

Cell Culture and Seeding

MC3T3-E1 cells (CRL-2594, ATCC) were used as the model cells in this research. Cells were cultured in alpha-modified minimum essential media (α-MEM, GENOM, China) supplemented with 10% fetal bovine serum (FBS, Cellmax, Australia) under a humidified atmosphere of 5% CO_2 at 37 ℃. Sub-confluent cells cultivated on tissue culture polystyrene (TCPS) were trypsinized using 0.25% trypsin/EDTA (Gibco) and suspended in fresh cell culture medium. Before cell seeding, the TiNR and Col/AuNPs were sterilized with an autoclave sterilizer (ZEALWAY, G154T) at 120 ℃ for 30 min and then transferred into a 24-wells plate. MC3T3-E1 cells were seeded on samples with a density of 1×10^5 cells mL^{-1} (500 μL) in cytocompatibility tests and 2×10^5 cells mL^{-1} in gene delivery experiment.

Cytocompatibility Tests of Composite Coating

Cell Adhesion and Proliferation Measurement Adhesion behaviors of MC3T3-E1 cells on both the TiNR and Col/AuNPs were evaluated after incubation for 1 day. The spreading morphology of cells were captured using an optical microscope and the number of adherent cells was counted with cell counting kit-8 (CCK-8, Dojingdo Laboratories, Kumamoto, Japan). Proliferation of MC3T3-E1 cells grown on different samples was quantified after culture for three days. For light illumination groups, cells were exposed to visible-light at an intensity of 150 mW cm^{-2} for 15 min after they were seeded on various composite coatings for 2 h. The OD values and morphology of cells grown on the composite coatings were characterized after 48 h of incubation.

ALP Activity Assay After 7-day and 14-day cultivation, different treated samples were transferred to new wells and washed three times with PBS. Then the biological cells were lysed using a cell lysis buffer (Sigma). ALP activity was quantified and normalized to total protein contents using a LabAssay ALP (Wako, Japan) and a protein kit (BCA, Thermo Scientific, U.S.A.). The ALP product of cells grown on different samples was stained using an ALP color development kit (Beyotime).

Quantitative Real-time PCR Assay The target gene expressions were measured using a real-time RT-PCR assay. The total RNA was extracted with TRIzol reagent and 500 ng of RNA was used to reverse-transcribe the cDNA. RT-PCR analysis was conducted on a Roche LightCycler480 system using SYBR Green as DNA dye. β-actin was used as the reference gene to normalize the relative expression of target genes. The primers used in this study are listed in Table 4.

Gene Delivery

To study the influence of visible-light illumination on cellular uptake of LF/GFP while excluding the interference of LF/GFP release, the conventional gene delivery experiment was firstly performed. Briefly, MC3T3-E1 cells were seeded on Col/AuNPs and incubated for 12 h to make cells fully attached to the surface. After that, LF/GFP were added into culture medium with a pEGFP concentration of 0.2 μg $well^{-1}$. Then the cells were exposed to the visible-light. Finally, GFP expression was assessed after cell culture for another 48 h. For surface-mediated gene delivery experiments, MC3T3-E1 cells were seeded on samples after LF/GFP immobilization. After cultivated for 2 h, cells were exposed to visible-light for 15 min at an intensity of 150 mW cm^{-2}. GFP expression efficiency and mean intensity of fluorescence were measured using the flow cytometry (Beckman, Cytoflex) and fluorescence microscope after culturing for another 48 h.

Cell Morphology Observations

In order to study the effect of visible-light illumination on cell cytoskeleton, F-actin was stained with fluorescent rhodamine conjugated phalloidin. Briefly, after culture for 12 h, MC3T3-E1 cells were treated with visible-light, and then immediately fixed with 4% paraformaldehyde (PFA) for 15 min. After that, cells were permeated with 0.4% Triton X-100 under room temperature for 15 min. F-actins were dyed with 50 μg mL^{-1} of phalloidin solution for 30 min and nucleus were stained with 5 μg mL^{-1} of 4'-6-diamidino-2'-phenylindole (DAPI) for 15 min at room temperature. Finally, cells were recorded using a laser confocal microscope (Zeiss, LSM780).

Statistical Analysis

All the tests were carried out in triplicate, and the obtained data were presented with mean value ± standard deviation (SD). Statistical analysis was performed through one-way variance analysis and Scheffe's post hoc test. Student's t-test was carried out using a Statistical Product and Service Solutions (SPSS) software. When p value was less than 0.05, the differences were considered as statistically significant (***$p<0.001$, **$p<0.01$, *$p<0.05$).

Conflicts of interest

The authors declare no conflict of interest.

Acknowledgements

This work was financially supported by the National Natural Science Foundation of China (NSFC 51872259, 31570962, 51772273), the 111 Project under Grant B16042, UK Engineering Physics and Science Research Council (EPSRC EP/P018998/1) and the Newton Mobility Grant (IE161019) through the Royal Society and NFSC.

References

ARTICLE

1. X. Z. Ren, J. X. Li, J. Y. Li, Y. Q. Jiang, L. Li, Q. Q. Yao, Q. F. Ke and H. Xu, *Chem. Eng. J.*, 2019, **370**, 1027-1038.
2. X. Z. Wang, Z. Chen, B. B. Zhou, X. Y. Duan, W. J. Weng, K. Cheng, H. M. Wang and J. Lin, *Acs Appl. Mater. Interfaces*, 2018, **10**, 11508-11518.
3. J. S. Fernandes, P. Gentile, R. A. Pires, R. L. Reis and P. V. Hatton, *Acta Biomater.*, 2017, **59**, 2-11.
4. S. Madduri, P. di Summa, M. Papaloizos, D. Kalbermatten and B. Gander, *Biomaterials*, 2010, **31**, 8402-8409.
5. W. Z. Chen, X. K. Shen, Y. Hu, K. Xu, Q. C. Ran, Y. L. Yu, L. L. Dai, Z. Yuan, L. Huang, T. T. Shen and K. Y. Cai, *Biomaterials*, 2017, **114**, 82-96.
6. P. S. P. Poh, D. W. Hutmacher, B. M. Holzapfel, A. K. Solanki, M. M. Stevens and M. A. Woodruff, *Acta Biomater.*, 2016, **30**, 319-333.
7. J. R. Jones, *Acta Biomater.*, 2013, **9**, 4457-4486.
8. R. Z. LeGeros, *Clin. Orthop. Rel. Res.*, 2002, 81-98.
9. Y. H. Youn, S. J. Lee, G. R. Choi, H. R. Lee, D. Lee, D. N. Heo, B. S. Kim, J. B. Bang, Y. S. Hwang, V. M. Correlo, R. L. Reis, S. G. Im and I. K. Kwon, *Mater. Sci. Eng. C-Mater. Biol. Appl.*, 2019, **100**, 949-958.
10. X. Y. Zhao, Y. Han, J. W. Li, B. Cai, H. Gao, W. Feng, S. Q. Li, J. G. Liu and D. S. Li, *Mater. Sci. Eng. C-Mater. Biol. Appl.*, 2017, **78**, 658-666.
11. D. Clark, X. Wang, S. Chang, A. Czajka-Jakubowska, B. H. Clarkson and J. Liu, *J. Biomed. Mater. Res. Part A*, 2015, **103**, 639-645.
12. K. A. White and R. M. Olabisi, *Adv. Healthcare Mater.*, 2019, **8**, 1801044.
13. H. Joo, J. Shin, S. W. Cho and P. Kim, *Adv. Healthcare Mater.*, 2016, **5**, 2025-2030.
14. J. Ziauddin and D. M. Sabatini, *Nature*, 2001, **411**, 107-110.
15. H. Jin, Z. S. Liu, W. Li, Z. L. Jiang, Y. Li and B. Zhang, *Rsc Adv.*, 2019, **9**, 26598-26608.
16. B. J. Zhang, L. He, Z. W. Han, X. G. Li, W. Zhi, W. Zheng, Y. D. Mu and J. Weng, *J. Mat. Chem. B*, 2017, **5**, 8238-8253.
17. M. Kang and C. Leal, *Adv. Funct. Mater.*, 2016, **26**, 5610-5620.
18. A. F. Adler and K. W. Leong, *Nano today*, 2010, **5**, 553-569.
19. J. C. Rea, R. F. Gibly, A. E. Barron and L. D. Shea, *Acta Biomater.*, 2009, **5**, 903-912.
20. C. X. He, N. Li, Y. L. Hu, X. M. Zhu, H. J. Li, M. Han, P. H. Miao, Z. J. Hu, G. Wang, W. Q. Liang, Y. Tabata and J. Q. Gao, *Pharm. Res.*, 2011, **28**, 1577-1590.
21. L. Tang, Y. Yang, T. Bai and W. G. Liu, *Biomaterials*, 2011, **32**, 1943-1949.
22. D. B. Peckys, A. V. Melechko, M. L. Simpson and T. E. McKnight, *Nanotechnology*, 2009, **20**, 145304.
23. T. Segura and L. D. Shea, *Bioconjugate Chem.*, 2002, **13**, 621-629.
24. Y. Yu, Y. Si, S. L. Bechler, B. Liu and D. M. Lynn, *Biomacromolecules*, 2015, **16**, 2998-3007.
25. C. Wang, L. Li, L. Ma, B. Li and C. Gao, *Journal of Bioactive and Compatible Polymers*, 2014, **29**, 221-234.
26. B. S. Aytar, M. R. Prausnitz and D. M. Lynn, *Acs Appl. Mater. Interfaces*, 2012, **4**, 2726-2734.
27. S. Mehrotra, I. Lee and C. Chan, *Acta Biomater.*, 2009, **5**, 1474-1488.
28. F. L. Callari, S. Petralia, S. Conoci and S. Sortino, *New J. Chem.*, 2008, **32**, 1899-1903.
29. F. Yamauchi, K. Kato and H. Iwata, *Langmuir*, 2005, **21**, 8360-8367.
30. X. F. Du, J. Wang, Q. Zhou, L. W. Zhang, S. J. Wang, Z. X. Zhang and C. P. Yao, *Drug Deliv.*, 2018, **25**, 1516-1525.
31. Z. Lyu, F. Zhou, Q. Liu, H. Xue, Q. Yu and H. Chen, *Adv. Funct. Mater.*, 2016, **26**, 5787-5795.
32. C. Luft and R. Ketteler, *J. Biomol. Screen*, 2015, **20**, 932-942.
33. R. Elnathan, B. Delalat, D. Brodoceanu, H. Alhmoud, F. J. Harding, K. Buehler, A. Nelson, L. Isa, T. Kraus and N. H. Voelcker, *Adv. Funct. Mater.*, 2015, **25**, 7215-7225.
34. A. Delalande, S. Kotopoulis, M. Postema, P. Midoux and C. Pichon, *Gene*, 2013, **525**, 191-199.
35. H. Zhang, J. Wang, M. Hu, B.-C. Li, H. Li, T.-T. Chen, K.-F. Ren, J. Ji, Q.-M. Jing and G.-S. Fu, *Biomater. Sci.*, 2019, **7**, 5177-5186.
36. J. Wang, K.-F. Ren, Y.-F. Gao, H. Zhang, W.-P. Huang, H.-L. Qian, Z.-K. Xu and J. Ji, *ACS Appl. Bio Mater.*, 2019, **2**, 2676-2684.
37. E. J. Ryan, A. J. Ryan, A. Gonzalez-Vazquez, A. Philippart, F. E. Ciraldo, C. Hobbs, V. Nicolosi, A. R. Boccaccini, C. J. Kearney and F. J. O'Brien, *Biomaterials*, 2019, **197**, 405-416.
38. Z. H. Liu, Y. Z. Li, W. Li, W. H. Lian, M. Kemell, S. Hietala, P. Figueiredo, L. Li, E. Makila, M. Ma, J. Salonen, J. T. Hirvonen, D. F. Liu, H. B. Zhang, X. M. Deng and H. A. Santos, *Mater. Horiz.*, 2019, **6**, 385-393.
39. T. Tenkumo, J. R. V. Saenz, K. Nakamura, Y. Shimizu, V. Sokolova, M. Epple, Y. Kamano, H. Egusa, T. Sugaya and K. Sasaki, *Mater. Sci. Eng. C-Mater. Biol. Appl.*, 2018, **92**, 172-183.
40. Y. H. Lee, H. C. Wu, C. W. Yeh, C. H. Kuan, H. T. Liao, H. C. Hsu, J. C. Tsai, J. S. Sun and T. W. Wang, *Acta Biomater.*, 2017, **63**, 210-226.
41. D. Cassano, M. Santi, F. D'Autilia, A. K. Mapanao, S. Luin and V. Voliani, *Mater. Horiz.*, 2019, **6**, 531-537.
42. X. M. Xu, X. M. Liu, L. Tan, Z. D. Cui, X. J. Yang, S. L. Zhu, Z. Y. Li, X. B. Yuan, Y. F. Zheng, K. W. K. Yeung, P. K. Chu and S. L. Wu, *Acta Biomater.*, 2018, **77**, 352-364.

43. S. Kang, J. Lee, S. Ryu, Y. Kwon, K. H. Kim, D. H. Jeong, S. R. Paik and B. S. Kim, *Chem. Mater.*, 2017, **29**, 3461-3476.
44. J. Das, Y. J. Choi, H. Yasuda, J. W. Han, C. Park, H. Song, H. Bae, J. h. Kim, *Sci. Rep.*, 2016, **6**, 33784.
45. C. Kojima, Y. Nakajima, N. Oeda, T. Kawano and Y. Taki, *Macromol. Biosci.*, 2017, **17**, 1600341.
46. L. M. Wang, B. B. Zhou, Z. G. Liu, L. Q. Dong, K. Cheng and W. J. Weng, *Colloids Surf. B Biointerfaces*, 2018, **167**, 213-219.
47. Z. Bengali, J. C. Rea, L. D. Shea, *J. Gene. Med.*, 2007, **9**, 668-678.
48. S. Modaresi, S. Pacelli, J. Whitlow, A. Paul, *Nanoscale*, 2018, **10**, 8947-8952.
49. B. K. K. Teo, S. H. Goh, T. S. Kustandi, W. W. Loh, H. Y. Low, E. K. F. Yim, *Biomaterials*, 2011, **32**, 9866-9875.
50. S. H. Hsu, T. T. Ho and T. C. Tseng, *Biomaterials*, 2012, **33**, 3639-3650.
51. X. Z. Wang, C. Yao, W. J. Weng, K. Cheng and Q. Wang, *Acs Appl. Mater. Interfaces*, 2017, **9**, 28250-28259.
52. J. M. Fleming, S. T. Yeyeodu, A. McLaughlin, D. Schuman, D. K. Taylor, *ACS Chem. Biol.*, 2018, **13**, 2825-2840.
53. F. Ge, M. F. Yu, C. X. Yu, J. Lin, W. J. Weng, K. Cheng and H. M. Wang, *Colloids Surf. B Biointerfaces*, 2017, **150**, 153-158.
54. D. Tang, K. Cheng, W. J. Weng, C. L. Song, P. Y. Du, G. Shen and G. R. Han, *Thin Solid Films*, 2011, **519**, 7644-7649.
55. K. Cheng, M. F. Yu, Y. Liu, F. Ge, J. Lin, W. J. Weng and H. M. Wang, *Colloids Surf. B Biointerfaces*, 2015, **126**, 387-393.
56. K. Belbachir, R. Noreen, G. Gouspillou and C. Petibois, *Anal. Bioanal. Chem.*, 2009, **395**, 829-837.

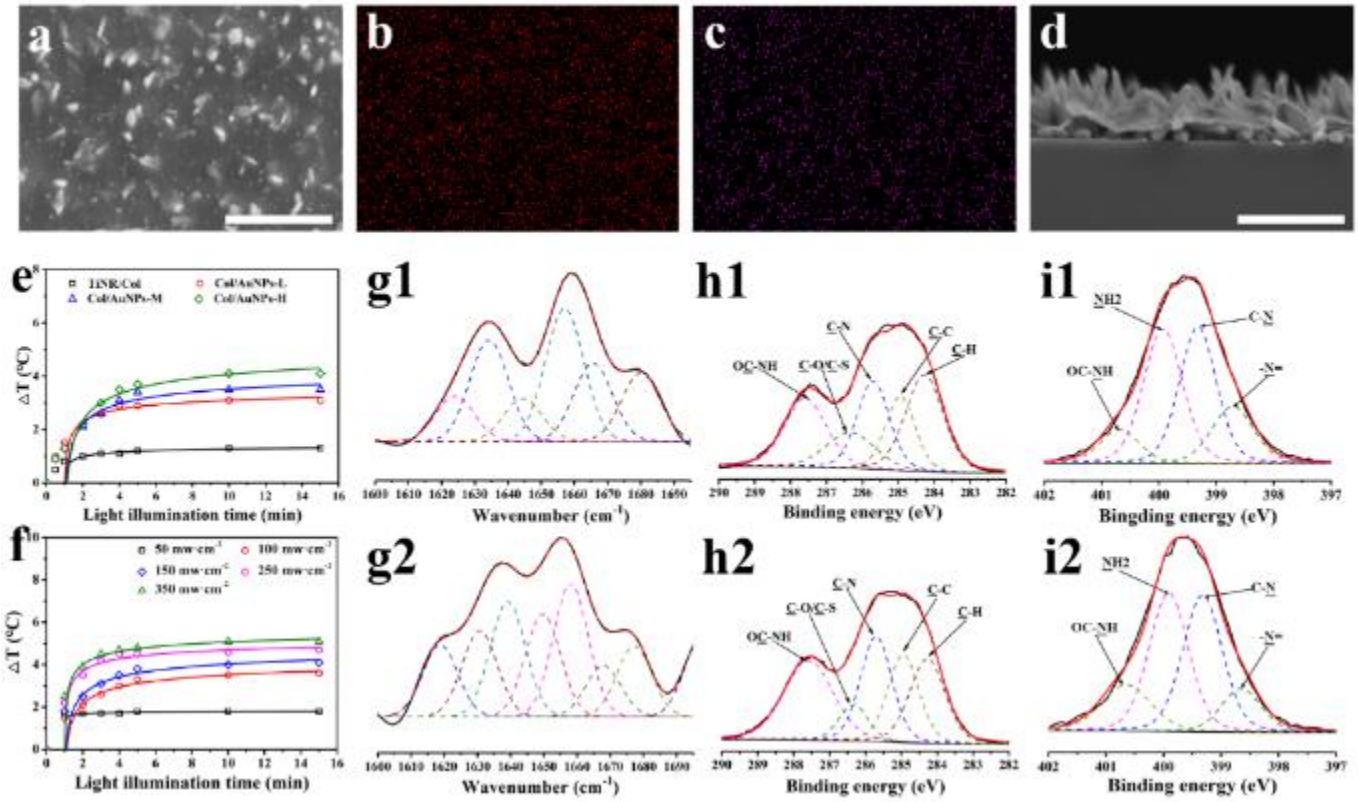

Figure 1. Characterization of Col/AuNPs composite coating. a) Topography of Col/AuNPs characterized by SEM, b) C element and c) Au element distribution of Col/AuNPs characterized by EDS, d) The cross section of Col/AuNPs, e) △T curve of samples with different gold nanoparticle contents as a function of light illumination time (light intensity:150 mW cm^{-2}). f) △T curve as a function of light illumination time at different light intensities (sample: Col/AuNPs-H). g) Peak fitting of amine Ⅰ region of collagen from FTIR spectra of Col/AuNPs g1) without light and g2) with light. h) C 1s and i) N 1s XPS spectra of Col/AuNPs h1) and i1) without light, h2) and i2) with light. Scale bar, 800nm.

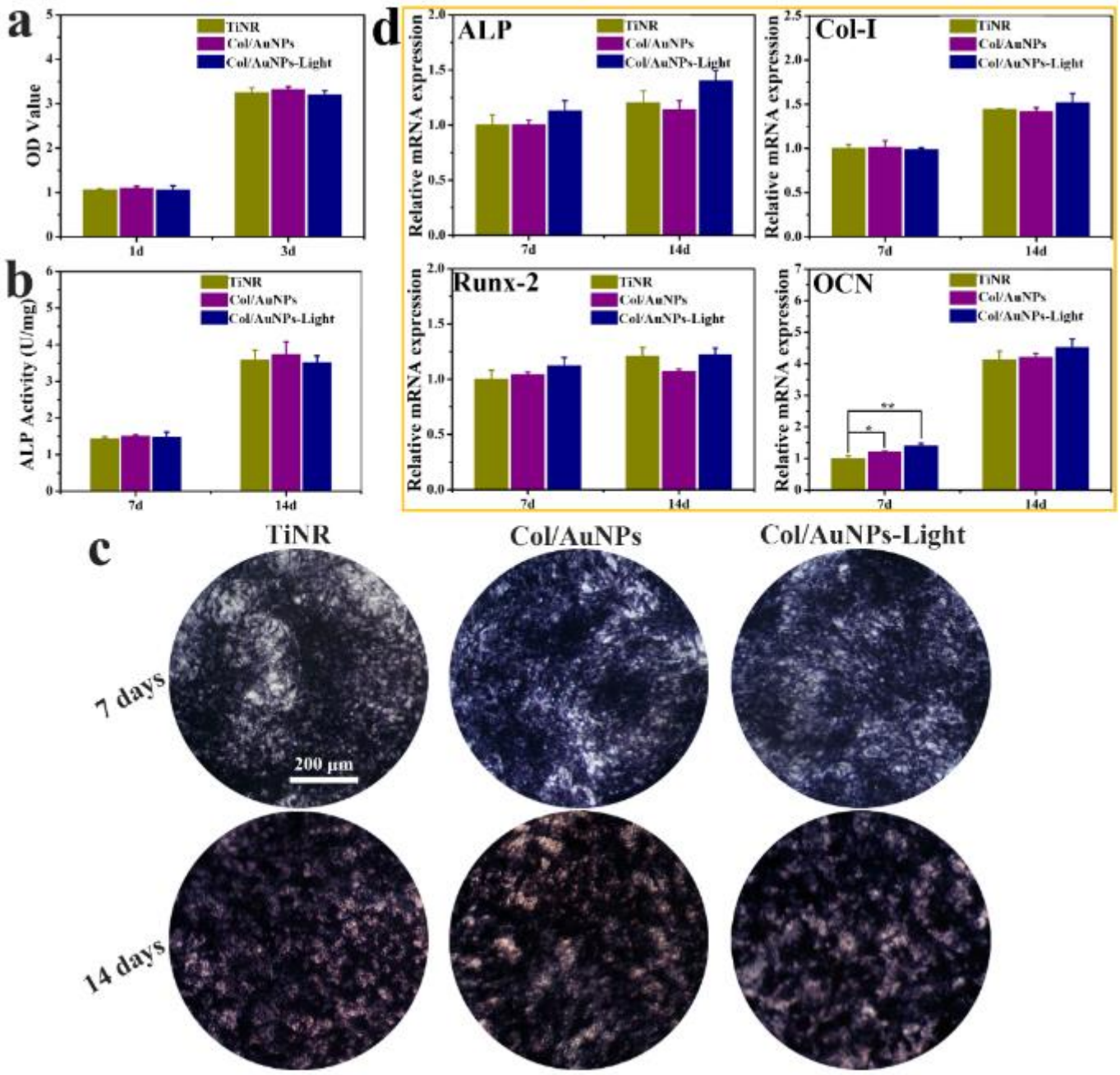

Figure 2. Cytocompatibility and osteogenic differentiation of Col/AuNPs composite coating. a) OD value b) ALP activity, c) The ALP staining images and d) the relative gene expression of ALP, Col- Ⅰ, Runx-2 and OCN of cells on various samples.

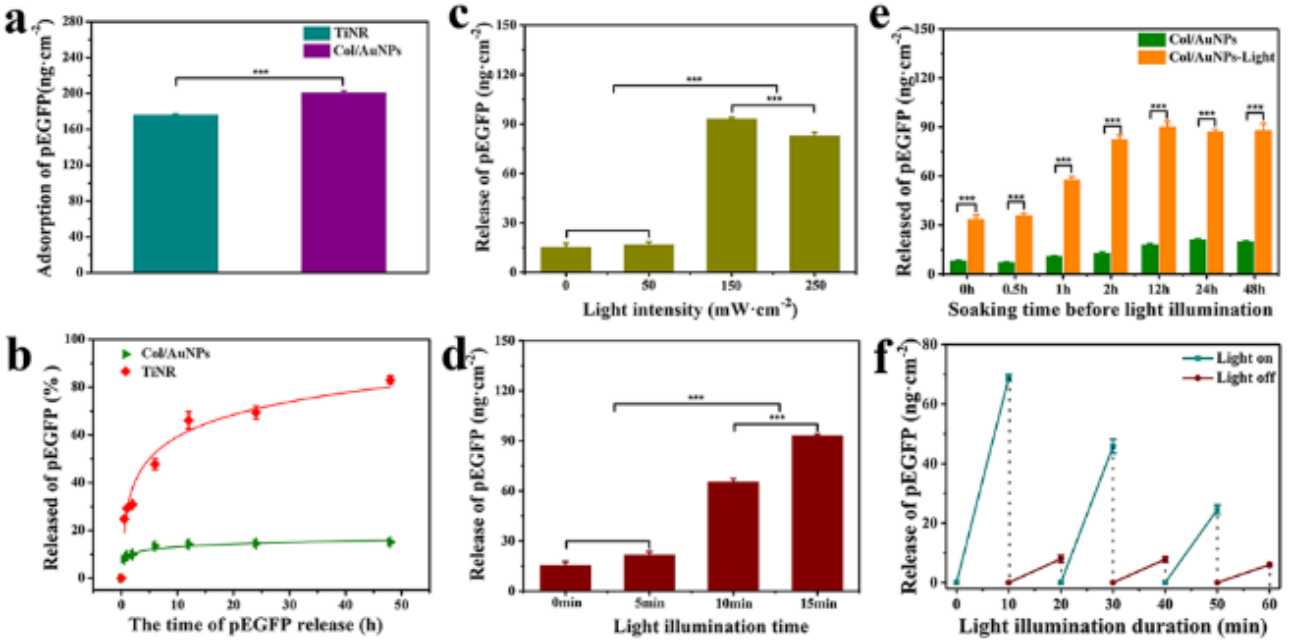

Figure 3. Immobilization and release of LF/GFP. a) Amount of pEGFP adsorption on different samples. b) Spontaneous release curve over time of pEGFP immobilized on different samples. Amount of pEGFP release from Col/AuNPs with different c) light intensity (illumination time: 15 min), d) illumination time (light intensity: 150 mW cm^{-2}) and e) with light treatment at different time point. f) Amount of pEGFP release from Col/AuNPs with periodic light on and light off (20 min for a cycle).

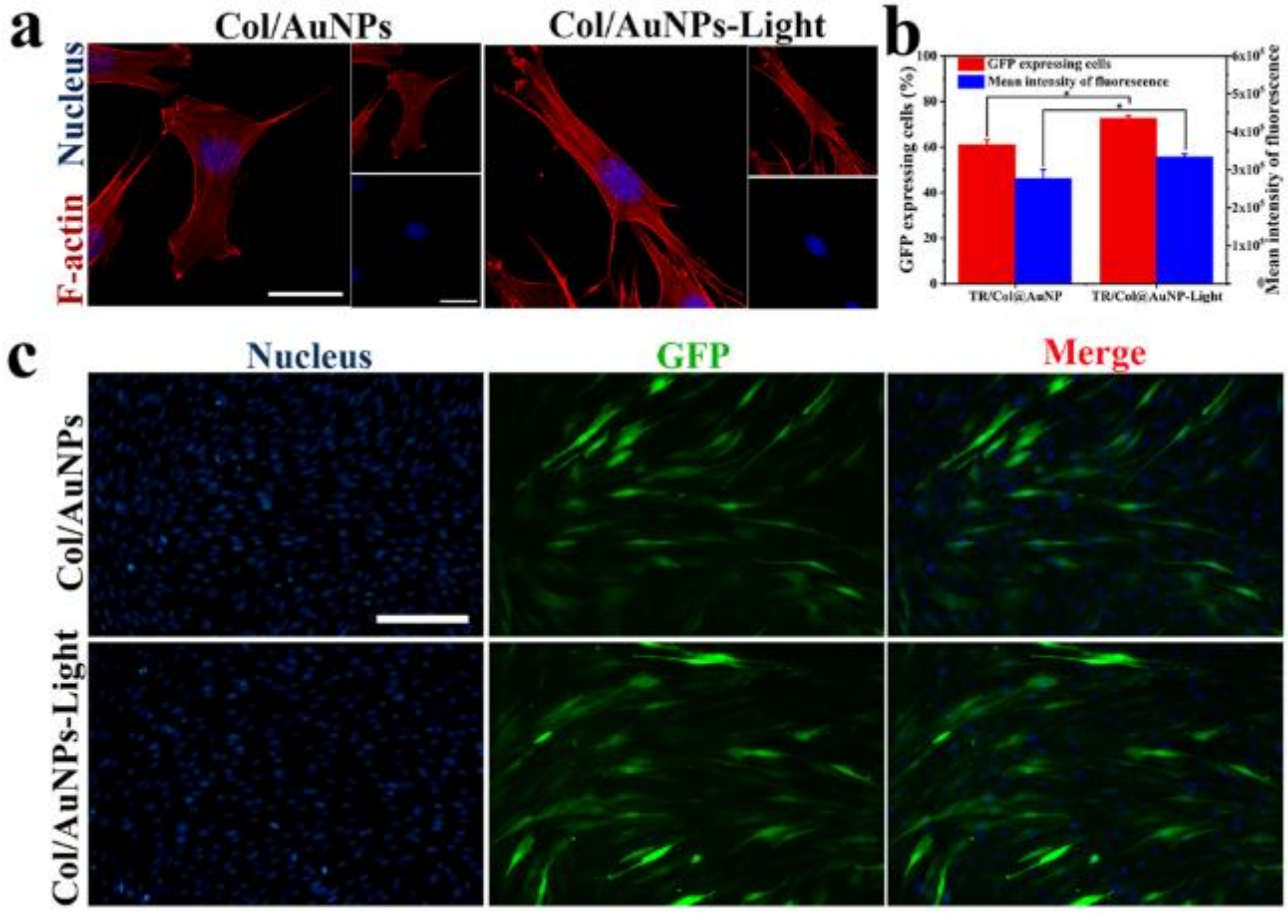

Figure 4. Visible-light promoted cellular uptake of LF/GFP. a) Laser confocal fluorescence microscopy analysis for cytoskeleton of cells cultivated on Col/AuNPs. b) GFP expression efficiency and mean fluorescence intensity of cells cultured on Col/AuNPs. c) GFP expression of cells cultured on Col/AuNPs characterized by fluorescence microscopy. Scale bar, 100μm.

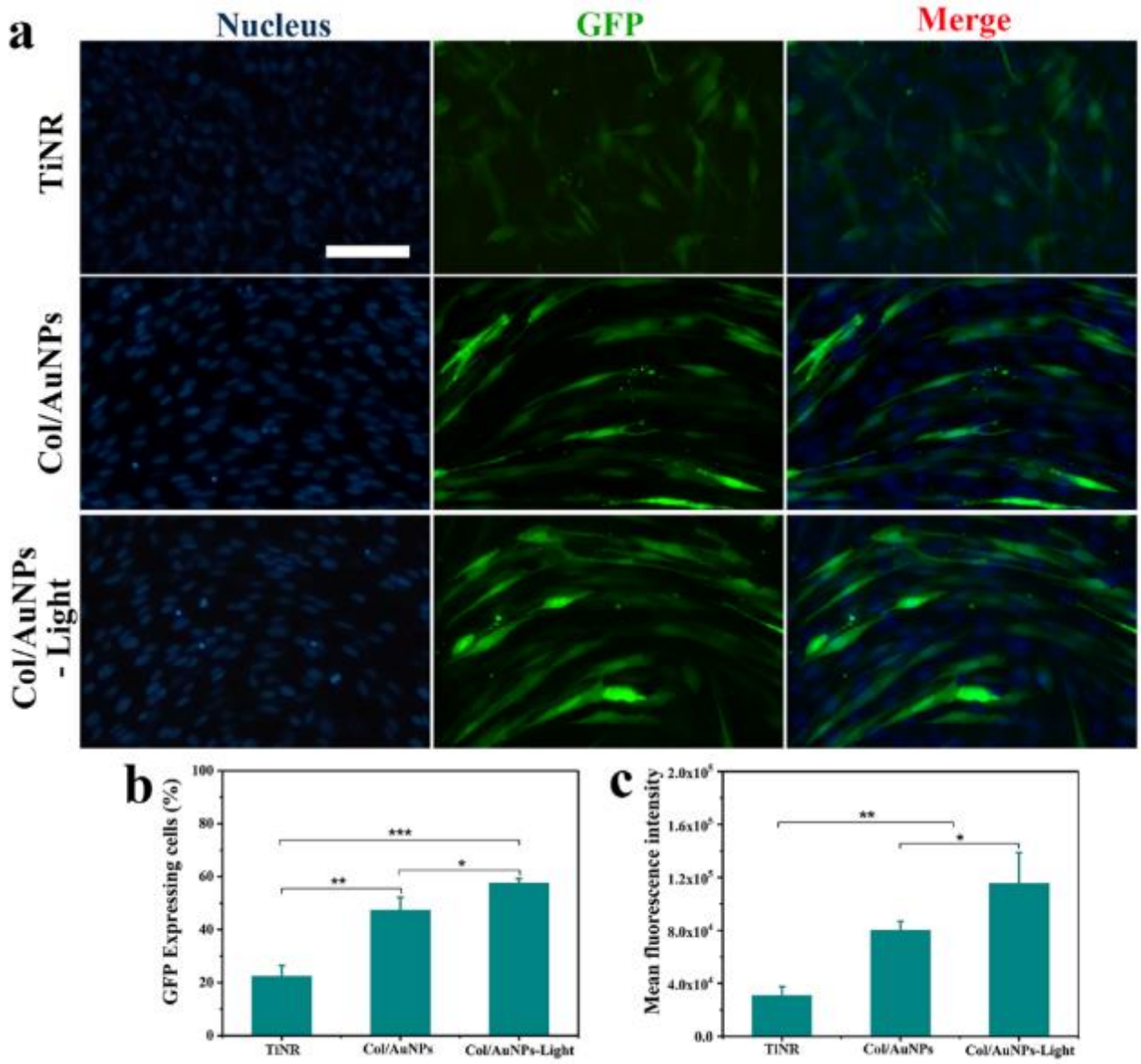

Figure 5. Visible-light promoted surface-mediated gene transfection. a) GFP expressing of cells grown on TiNR and Col/AuNPs characterized by a fluorescence microscope, flow cytometry analysis for b) transfection efficiency in percentage of total cell population and c) mean fluorescence intensity of transfected cells cultured on TiNR and Col/AuNPs. Scale bar, 50µm.

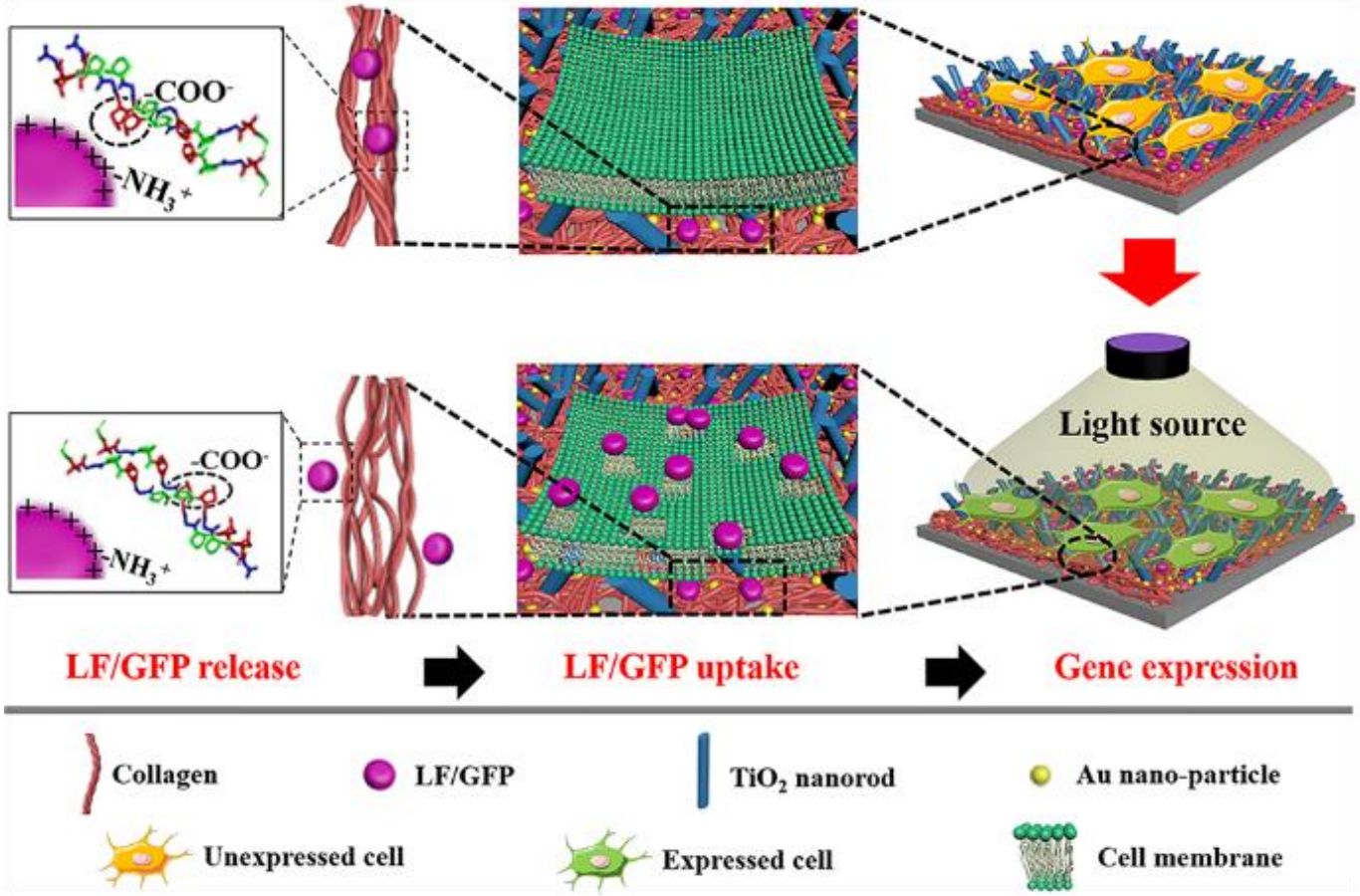

Figure 6. Schematic illustrations of effect of visible-light illumination on Col/AuNPs mediated gene delivery.

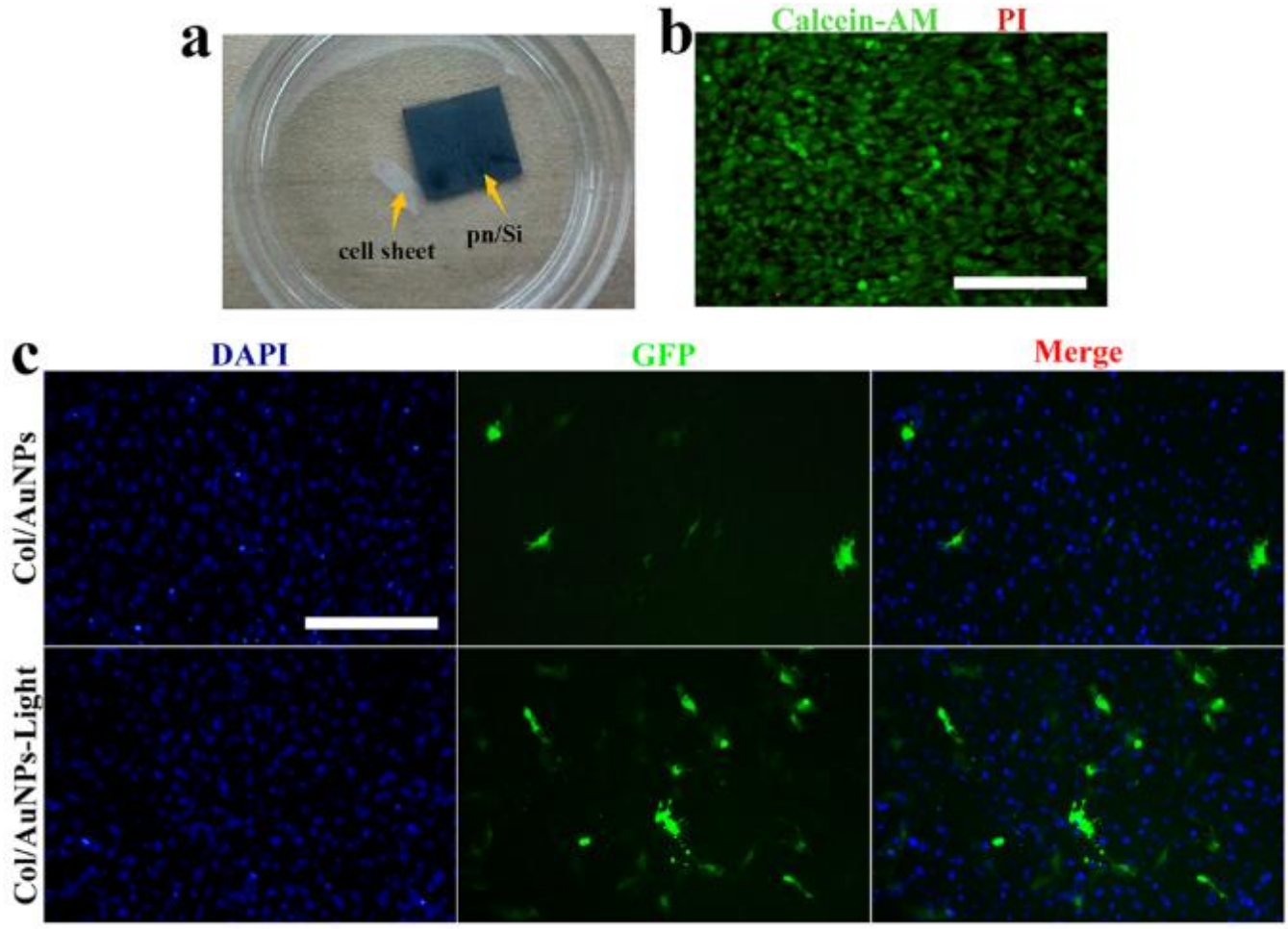

Figure 7. Viability and GFP expression of cell sheet. a) Image of cell sheet detached from Si. b) Viability and c) GFP expression of cell sheets replanting on Col/AuNPs composite coating. Scale bar, 200μm.

Table 1. Secondary structure content of Col-Ⅰ before and after light illumination characterized by FTIR spectra

	Secondary structure (%)					
	Side chains	Triple helix	unordered	β-turn	α-helix	β-sheet
W/O light		21.6	9.1	16.7	28.3	24.3
W/ ligth	10.1	16.1	14.4	18.7	18.7	22.0

Table 2. Contents of C-containing group of Col/AuNPs before and after light illumination analyzed by XPS

	C-containing group and relative area (%)				
	OC-NH	C-O/C-S	C-N	C-C	C-H
Col/AuNPs	21.5	13.2	21.3	16.5	27.5
Col/AuNPs-Light	27.9	7.6	23.6	19.6	21.3

Table 3. Contents of N-containing group of Col/AuNPs before and after light illumination analyzed by XPS

	N-containing group and relative area (%)			
	OC-NH	NH2	C-N	-N=
Col/AuNPs	8.5	39.9	34.6	17.0
Col/AuNPs-Light	14.0	38.0	36.7	11.3

Table 4. Primers used in RT-PCR.

Gene	forward primer sequence (5′-3′)	reverse primer sequence (5′-3′)
ALP	CCAGAAAGACACCTTGACTGTGG	TCTTGTCCGTGTCGCTCACCAT
Col-Ⅰ	CCTCAGGGTATTGCTGGACAAC	CAGAAGGACCTTGTTTGCCAGG
Runx-2	CCTGAACTCTGCACCAAGTCCT	TCATCTGGCTCAGATAGGAGGG
OCN	GCAATAAGGTAGTGAACAGACTCC	CCATAGATGCGTTTGTAGGCGG
β-actin	AATGTGGCTGAGGACTTTG	GGGACTTCCTGTAACCACTTATT